NIH Public Access
Author Manuscript
Mutat Res. Author manuscript; available in PMC 2009 December 15.

Published in final edited form as:
Mutat Res. 2008 December 15; 648(1-2): 23–31. doi:10.1016/j.mrfmmm.2008.09.006.

RAD18 and associated proteins are immobilized in nuclear foci in human cells entering S-phase with ultraviolet light-induced damage

Nicholas B. Watson[1], **Eric Nelson**[2], **Michelle Digman**[3], **Joshua A. Thornburg**[1], **Bruce W. Alphenaar**[2], and **W. Glenn McGregor**[1,4]

1 *Department of Pharmacology and Toxicology and James Graham Brown Cancer Center, University of Louisville, Louisville, KY 40202*

2 *Department of Computer and Electrical Engineering, University of Louisville, Louisville, KY 40202*

3 *Laboratory for Fluorescence Dynamics, University of California, Irvine, CA 92697*

Abstract

Proteins required for translesion DNA synthesis localize in nuclear foci of cells with replication-blocking lesions. The dynamics of this process were examined in human cells with fluorescence-based biophysical techniques. Photobleaching recovery and raster image correlation spectroscopy experiments indicated that involvement in the nuclear foci reduced the movement of RAD18 from diffusion-controlled to virtual immobility. Examination of the mobility of REV1 indicated that it is similarly immobilized when it is observed in nuclear foci. Reducing the level of RAD18 greatly reduced the focal accumulation of REV1 and reduced UV mutagenesis to background frequencies. Fluorescence lifetime measurements indicated that RAD18 and RAD6A or polη only transferred resonance energy when these proteins colocalized in damage-induced nuclear foci, indicating a close physical association only within such foci. Our data support a model in which RAD18 within damage-induced nuclear foci is immobilized and is required for recruitment of Y-family DNA polymerases and subsequent mutagenesis. In the absence of damage these proteins are not physically associated within the nucleoplasm.

Keywords

RAD18; REV1; DNA polymerase eta; UV mutagenesis; FLIM/FRET; RICS

Introduction

Most mutations induced by carcinogens occur when DNA containing residual damage is replicated during S-phase of the cell cycle. Such lesions perturb the structure of DNA and are likely to block replicative DNA polymerase complexes. Knowledge of fundamental mechanisms involved in the replication of damaged genomes, and of the factors that determine if this process will be error-free or error-prone, is likely to be useful in elucidating the origins

4To whom correspondence should be addressed: 221A Baxter I Biomedical Research Building, 570 S. Preston Street, Louisville, KY 40202, Tel: 502-852-2564, Fax: 502-852-2492, Email: wgmcgregor@louisville.edu.

Publisher's Disclaimer: This is a PDF file of an unedited manuscript that has been accepted for publication. As a service to our customers we are providing this early version of the manuscript. The manuscript will undergo copyediting, typesetting, and review of the resulting proof before it is published in its final citable form. Please note that during the production process errors may be discovered which could affect the content, and all legal disclaimers that apply to the journal pertain.

NIH-PA Author Manuscript
NIH-PA Author Manuscript
NIH-PA Author Manuscript

NIH-PA Author Manuscript

NIH-PA Author Manuscript

NIH-PA Author Manuscript

of cancer and other human diseases. Originally examined in budding yeast, Lawrence and colleagues determined that replication-blocking lesions in the template strand can be bypassed by proteins in the RAD6 DNA damage tolerance pathway [1]. Replication of the damaged template is completed by translesion synthesis (TLS) with potentially mutagenic consequences, or by damage avoidance mechanisms mediated by recombination that are largely error-free [2]. These mechanisms are conserved but with additional layers of complexity in higher eukaryotes [3;4]. The ubiquitin conjugating enzyme RAD6 and the associated ligase RAD18 are central to this process. Mutants cannot bypass replication-blocking lesions in the template and are sensitive to many DNA damaging agents. Proliferating cell nuclear antigen (PCNA) ubiquitinated at K164 by the RAD6/18 complex signals TLS [5] and further ubiquitination may signal damage avoidance, although the mechanisms involved in the latter error-free process are poorly understood [3]. Data indicate that PCNA ubiquitinated at K164 has increased affinity for the Y-family polymerases, notably polη and polι [6;7]. Two other members of the Y-family, REV1 and polκ, also contain novel ubiquitin-binding domains [7]. The ubiquitin-binding domain of REV1 is required for functional interaction with PCNA and damage-induced mutagenesis [8], but the catalytic domain of REV1 is dispensable [9]. The principal function of REV1 in TLS is presumably structural since the protein interacts with other Y family polymerases and with REV7 [10]. The latter protein is a subunit of the B-family polymerase ζ. [11–13]. In addition to the well-established requirement for RAD18 in the resolution of blocked DNA replication forks, RAD18 has been shown to form nuclear foci in synchronized cells irradiated in G_1, G_1/S, or G_2 phases of the cell cycle [14]. The function of the protein under these circumstances is unknown, but may be related to a physical interaction of RAD18 with RPA coating single stranded regions of DNA [15].

We examined the intranuclear dynamics of the DNA damage response of a RAD18-eGFP fusion protein in living human cells using a variety of fluorescence dynamics techniques. The fusion protein accumulated in nuclear foci in a small percentage of cells that were undamaged, but the frequency of cells with nuclear foci increased over 10-fold 4 hours after UV-irradiation. The increase in the percentage of cells with nuclear foci was strictly dependent on S-phase, since examination of synchronized cells indicated that this increase only occurred in populations that were irradiated at the beginning of S-phase. These foci exhibited a reduction in redistribution after photobleaching, which was quantified by raster image correlation spectroscopy (RICS). Damage-induced focal immobilization of REV1-eGFP was dependent on RAD18. Cells with reduced levels of the latter protein formed foci with a greatly reduced frequency and had slightly enhanced cytotoxic but greatly reduced mutagenic responses to UV. Fluorescence lifetime measurements (FLIM) indicated that RAD18 transferred Förster resonance energy (FRET) to RAD6A or to polη only when the proteins colocalized in damage-induced nuclear foci. This indicates that these proteins are in close physical association only within such foci. These data support a model in which RAD18 is immobilized within damage-induced nuclear foci and is required for subsequent recruitment of proteins required for TLS.

Materials and Methods

Cells and cell culture

The primary fibroblast cell strain GM1604 (Coriell Institute) was originally derived from human fetal lung tissue. The telomerase immortalized cells (NF1604) [16] were a generous gift of Dr. Lisa McDaniels (University of Texas Southwestern Medical Center, Dallas) under the terms of MTA 3025 between WGM and Geron Corporation. Cells were kept in exponential growth using published conditions [17].

NIH-PA Author Manuscript

NIH-PA Author Manuscript

NIH-PA Author Manuscript

Construction of plasmids

The coding sequence of RAD18 was amplified by PCR using the DNA from plasmid pEGLha-hRAD18 [18]. EcoR1 and BamH1 restriction sites were added to the ends of the open reading frame of RAD18. The DNA was ligated into the EGFP-N2 vector (Clontech), such that the fusion protein consists of RAD18 fused with eGFP at the C-terminus of RAD18 (RAD18-eGFP). A PCR product that encoded RAD18 was ligated into pcDNA3 (Invitrogen) in the antisense orientation, for knockdown studies.

For FLIM/FRET studies the coding region for RAD18 was cloned into pAmCyanC1 (Clontech), which expresses CFP fused in-frame with the N-terminus of RAD18. The coding sequences for RAD6A and polη were obtained by reverse-transcription-PCR using total RNA extracted from primary human fibroblasts and cloned into pZsYellow-C1 (Clontech). The latter fusion proteins have YFP fused to the N-terminus of the protein of interest. A plasmid encoding full-length REV1 (base pairs 1–3753) with eGFP fused to the C-terminus of REV1 was constructed as described [19].

All plasmids were sequenced to verify that no mutations had been introduced in the cloning process and that the coding regions were in frame.

Plasmid transfection and cell synchronization

Electroporation of plasmids was done using the system from Amaxa Biosystems (Amaxa Inc, Gaithersburg, MD) with proprietary reagents and conditions provided by the manufacturer, and as described previously [17;19]. Electroporation reduced cell viability by approximately 10% as determined by clonogenic assays. Following electroporation, cells were cultured for 36 hours in complete media to achieve plating and protein expression. Mimosine (0.5 mM final concentration, Sigma, USA) was added to the culture medium for 24h under low serum conditions (0.1% FBS), after the cells had attached. At this point, the medium was changed, omitting mimosine. To determine the percentage of cells in G_1-, S- or G_2/M-phases of the cell cycle, an aliquot of the cells was trypsinized immediately, 6 hours or 12 hours after the block was removed. These cells were fixed and stained with propidium iodide. The DNA content was examined with flow cytometry.

UV- induced cytotoxicity

Cells were plated at cloning density the day before irradiation on 10 cm dishes. The UV source was a Spectroline germicidal lamp, and the flux was measured at 254nm using a research radiometer fitted with a SED240 photodetector and a W diffuser (International Light, Newburyport, MA, USA). Irradiation was performed as described [17]. The medium was changed 1 week after irradiation, and the cells were stained with crystal violet after two weeks.

Western blot

Cells were collected at ~80% confluence from 15 cm cell culture dishes in lysis solution (10 mM Tris pH 7.4, 1 mM EDTA, 0.1% SDS, and 180 μg/ml PMSF). The solutions were centrifuged at 14,000 × g for 30 min at 4°C. The supernatants were collected and the protein concentrations were determined. Ten μg (RAD18) or 30 μg (PCNA) of whole cell extracts were electrophoresed on 12% SDS-PAGE gels. Following transfer to PVDF filters, the blots were probed with 1:500 mouse anti-RAD18 (Imgenex, San Diego, CA, USA or Abcam, Cambridge, MA, USA) or 1:1000 mouse anti-PCNA (Abcam) and 1:10,000 mouse anti-β actin (Sigma). Horseradish peroxidase (Zymed) was used at a dilution of 1:10,000.

NIH-PA Author Manuscript

NIH-PA Author Manuscript

NIH-PA Author Manuscript

Determination of the mutagenic effects of UV

A series of independent populations of cells were synchronized by density-inhibition/serum starvation as described [20]. Each population of 1.5×10^6 cells was irradiated 17 h after release from confluence, which corresponds to ~1 h after the onset of S phase. For irradiation, the culture medium was aspirated, and the cells were washed with sterile PBS (pH 7.4). The cells were irradiated as described previously [20] with 8 J/m^2 of $UV_{254\ nm,}$ or sham-irradiated. Clonogenic survival was determined, and resistance to thioguanine was examined after an 8 day expression period as described [17].

Fluorescence recovery after photobleaching (FRAP)

The technology underlying the examination of the redistribution of fluorescently-tagged proteins in living cells depends upon extinguishing the fluorescence of those proteins with an intense laser pulse. This is done in a region of the cell, in this case the nucleus, that is small with respect to the size of the organelle. Proteins that are freely diffusible within the nucleoplasm are detected within the bleached area in several milliseconds. In contrast, constrained proteins do not, such that the bleached area remains so on a time scale of that can be orders of magnitude longer. To conduct these measurements on RAD18-eGFP or REV1-eGFP fusion proteins, cell fluorescence was observed with an inverted Olympus BX-51 microscope illuminated with a filtered Hg arc-lamp. To locally bleach the eGFP, spatially filtered light from an Ar ion laser with a wavelength of 488 nm and a power of 100 mW was focused on the cell. A bleaching pulse of less than 0.5 seconds in duration was used with a spot size of approximately 1.5 microns in diameter. Following bleaching, the fluorescence signal was monitored continuously within the bleached spot. A Perkin-Elmer Single Photon Counting Module, Series SPCM-AQR was used. This provides highly sensitive measurements of the fluorescence intensity coming from a 1 micron diameter region of the cell. Fluorescence images of the entire cell can be obtained by scanning the cell with respect to the detector using a piezoelectric drive stage. Post-bleach fluorescent intensity values were normalized to pre-bleach levels, and data from ten cells of each tested variety were averaged to produce the results presented here.

Raster image correlation spectroscopy (RICS)

This technology is based upon the movement of fluorescent proteins into and out of a confocal plane over time. The reason for doing this is to accurately determine diffusion coefficients of fluorescently-labeled proteins within living cells. The confocal image of the cell is scanned with the excitatory laser first in the X-direction (microsecond scale), and repeated line-by line (millisecond scale). This process defines raster imaging. One hundred images are recorded sequentially such that the movement of the protein over two minutes is recorded. A rapidly moving protein in the confocal plane will be detected in the X direction and perhaps the Y direction, but will not be detected in subsequent images taken over time. The converse will be true of a constrained protein. To conduct these experiments, cells were irradiated with either 10 J/m^2 UV_{254nm} or sham irradiated 24h after transfection. Confocal images were collected 4 hrs after UV exposure on a XI81 inverted Olympus Fluoview 1000 microscope. A 60xW UPLSAPO objective (1.20 NA) water immersion objective was used to acquire all the images, which were obtained with an Ar ion laser using the 488nm laser line (Melles Griot, Tokyo, Japan) attenuated to 750V. A dichroic filter(DM 488/543/633) was used for the laser excitation and for collection of the emission. A bandpass filter (BA 505–605) was selected for eGFP-labeled cells. Images were collected using the Fluoview software with a pixel resolution of 0.03 mm at 256×256 pixels with a pixel dwell time of 12.5 μs/pixel. Diffusion coefficients were determined using SimFCS imaging analysis software [21].

NIH-PA Author Manuscript

NIH-PA Author Manuscript

NIH-PA Author Manuscript

Fluorescence lifetime measurements (FLIM)

Cells were transiently transfected with RAD18-CFP, RAD18-CFP + RAD6A-YFP, or RAD18-CFP + polη-YFP. Cells were irradiated with either 10 J/m^2 UV_{254nm} or sham irradiated. Images were collected on a Zeiss Axiovert S100TV microscope 4 hrs after UV exposure. A 60xW UPLSAPO objective (1.20 NA) water immersion objective was used to acquire all the images. A Ti:Sapphire laser attenuated to 820nm was used. FLIM data were collected with a Becker and Hickl card model 830 TCSPC. Only the donor emission was measured with a band pass filter (centered at 474±15 nm from Chroma Technologies, Battleboro, NJ) as well as a dichroic mirror (505DCXR, Chroma Technologies). This filter combination produces negligible bleedthrough for the emission of the YFP into the donor channel. SimFCS imaging analysis software (Globals for Images, Champagne, IL) was used to analyze images and calculate FRET efficiency [22].

Results

S-phase dependence of damage-induced nuclear foci

RAD18 forms distinct nuclear foci that colocalize with PCNA and Y-family polymerases in less 5% of cells that are not exposed to exogenous DNA damaging agents. The nature of these foci in cells that have not been exposed to genotoxic agents is a matter of conjecture. As shown in Fig. 1A, mimosine results in a G_1 block in which 70% of the cells are in this phase. Six hours after removal of the mimosine, flow data (not shown) indicate that the population remains in G_1. Irradiation of the synchronized cells shortly after release and examined with confocal microscopy 4 hours later when they are still in G_1 indicates that there is no increase in the percentage of cells with nuclear foci. Fig. 1B shows the distribution of RAD18-eGFP in unirradiated cells, and Fig. 1C in cells irradiated and examined 4h later. There is no increase in the percentage of cells with nuclear foci. The fraction of such cells increases greatly after exposure to UV [23;24], and this increase only occurs when the cells are irradiated at the beginning of S. Fig. 1D shows the cell cycle profile of cells 12 hours after release, at which point most of the population is in S-phase. Fig. 1E is a confocal image characteristic of RAD18-eGFP in synchronized cells that have not been irradiated, and 1F, the focal pattern in cells 4 hours after irradiation at the beginning of S-phase. The focal pattern is found in the great majority of cells in this situation, supporting the conclusion that these foci represent stalled replication foci.

Fluorescence redistribution after photobleaching (FRAP)

We examined the dynamics of RAD18-eGFP nuclear localization in living cells in response to UV damage. We determined the rate of fluorescence redistribution in cells that were undamaged, cells that were exposed to UV but did not exhibit a focal nuclear pattern, and cells that were UV-damaged and did exhibit a focal nuclear relocalization of the fusion protein. Fig. 2H shows the results for 10 cells in each group. All data points are shown, and the black lines represent the mean I/I_0 as a function of time after photobleaching. The slight differences in the initial photobleach represented on the Y-axis are due to minor differences in the initial laser pulse, and do not affect the rate of fluorescence redistribution. The top line (□) is the rate of redistribution for undamaged cells, and shows that there is rapid redistribution after the bleaching pulse. The data in the middle line (X) represent the redistribution in damaged cells that did not have a focal nuclear pattern. The rates of redistribution, I/I_0 ratios of 0.2 to 0.19 respectively, under these conditions are indistinguishable from each other and from that of eGFP alone (data not shown). Visual inspection confirmed that fluorescence intensity of control cells did not fully return to pre-bleach levels due to bleach-induced global reduction of fluorescence rather than partial protein immobility. In contrast, data in the bottom line (Δ) indicate that there is little recovery of the RAD18-eGFP signal in damage-induced nuclear foci

NIH-PA Author Manuscript

NIH-PA Author Manuscript

NIH-PA Author Manuscript

with an I/I_0 ratio of 0.08. These results support the idea that RAD18 is not present in preformed complexes, but becomes immobilized within the foci subsequent to DNA damage.

Raster image correlation spectroscopy (RICS)

The apparent lack of fluorescence relocalization of focal RAD18 indicated in the FRAP experiments was quantified using RICS. Analyzed with SimFCS software, cumulative data from the raster scanning images of the diffusion coefficients of RAD18-eGFP in 10 undamaged cells without foci (Fig 2 A, B) and 10 cells irradiated with $10J/m^2$ UV_{254nm}-induced nuclear foci (Fig 2 D, E) are shown. Fluorescence intensity is indicated and ranges from blue (low) to red (high). Figs. 2C and 2F are the two dimensional spatial correlation maps corresponding to 2B and 2E respectively. In undamaged cells, RAD18-eGFP was found to be freely mobile in the nucleus with an average diffusion coefficient of ~$13\mu m^2$/sec (Fig 2G left column). This compares with eGFP in the nucleus, which has a diffusion coefficient of $21\mu m^2$/sec [25]. This rapid movement yields a spatial correlation that extends only in the x-direction of the spatial correlation function as indicated in the circle in Fig 2C. Since RAD18 is free to diffuse in any direction, the fluorescent signal was detected in a few pixels along the line of scanning and then lost as the scan progresses onto the next line. In damaged-induced foci observed in cells 4h after UV, the diffusion coefficient was reduced 75% to ~$3\mu m^2$/sec (Fig 2G right column). This is reflected in the broad spatial correlation coefficient of fluorescence in the foci (Fig 2F). The high degree of correlation indicates that RAD18-eGFP in the foci cannot diffuse out of the confocal plane within the time frame (2 min) of the serial raster images. The average overall diffusion coefficient in cells examined 30 min after UV was $12.3\mu m^2$/sec (Fig 2G middle column). At this early time point, a few cells were found to have nuclear foci in which the protein was immobilized but the majority of cells exhibited undamaged diffusion coefficients.

Fluorescence lifetime imaging microscopy (FLIM)

FLIM is a simple yet reliable technique used to measure fluorescence resonance energy transfer (FRET) between two closely associated molecules. FRET from FLIM data is measured not by the traditional method of exciting the donor at one wavelength and measuring the increase in fluorescence of the acceptor at a separate wavelength, but rather by examining the decrease in donor fluorescence lifetime in the presence of the acceptor. Recent advances have resulted in an improved method to calculate FRET from FLIM data using the phasor plot [22]. This is particularly useful when the lifetime of the donor is not a single exponential, which is the case for the fluorescent proteins.

Figure 3 column 1 (from top to bottom) shows a cell expressing RAD18-CFP in the absence of the acceptor without UV irradiation, the intensity image, the pixel's selection (highlighted in pink) corresponding to the phasors selected by the black circle in the phasor plot and the average lifetime (obtained by intercepting the universal circle with a line starting at the origin and passing through the center of the selected phasor region [22]). Column 2 shows a cell co-transfected with RAD18-CFP/RAD6-YFP before UV irradiation. The black circle in the phasor plot selects these pixels in the image shown in the selection row and corresponding to the black part of the lifetime histogram. Column 3 shows a cell co-transfected with the RAD6A-YFP construct after irradiation. The bright fluorescence spots in the intensity image have a shorter lifetime as shown in the phasor plot. The shortening of the lifetime is such that the decay is shorter than the decay of the autofluorescence (data not shown), indicating that FRET is occurring. To calculate the FRET efficiency we used the method as described in Digman *et al.* [22]. Briefly, due to the presence of the acceptor, the phasor of the donor can be found along an ellipsoidal trajectory (black line in the column 2–3 inset) corresponding to FRET efficiency from 0 to 100%. The zero point is found by using the linear combination of the phasor of the (unquenched) donor with the phasor of the autofluorescence independently measured in column 1. The FRET trajectory intersects the cluster of phasors shown inside the red circle.

NIH-PA Author Manuscript

NIH-PA Author Manuscript

NIH-PA Author Manuscript

The position of this circle along the trajectory provides the FRET efficiency. For these constructs we found that the FRET efficiency was 72%, whci was consistently observed in the analysis of foci in 20 cells.

Figure 3 column 4 shows a representative image of a cell co-transfected with the RAD18-CFP and polη-YFP expression vectors, in the absence of UV damage. FRET is not observed. Column 5 is representative cells co-transfected with the same constructs, 4h after UV irradiation. In this case we observe FRET, and the analysis of the FRET trajectory also gives a value of 72% for the efficiency. This efficiency was consistently observed in 20 cells.

Construction of cell strains with reduced expression of RAD18

NF1604 cells transfected with an antisense RNA construct were screened for RAD18 protein expression (Fig. 4A). The clone with the lowest RAD18 protein levels was clone 26 (AS26), which had an 85% reduction in protein. To ensure that this reduction was functionally significant, ubiquitination of PCNA (PCNA-ubi) was examined. Cells were irradiated with 0 or 15J/m^2 UV_{254nm}. Western analysis (Fig. 4B) indicated that the parental cell line had a second band induced by UV that has been shown to be PCNA-ubi [5;6]. In contrast, this band is greatly reduced in AS26 cells, consistent with a lack of RAD18 function. AS26 was chosen for further examination of the role of RAD18 in mutagenesis and recruitment of REV1.

Reduced expression of RAD18 results in greatly reduced mutant frequencies induced in *HPRT* by UV

The cells with reduced RAD18 consistently exhibited moderately enhanced sensitivity to UV compared with the parental cells, but this did not achieve statistical significance. The UV fluence required to reduce the survival to 37% of the unirradiated controls (i.e., LD_{37}) was 7.0 J/m^2 for the parental cells and 5.5 J/m^2 for AS26 (data not shown).

In preliminary experiments, the mutant frequency induced in the *HPRT* gene was determined in AS26 cells and compared with the parental cell line NF1604. In asynchronously growing cells, mutations induced by UV in AS26 cells were consistently reduced to background levels. In order to minimize the effect of nucleotide excision repair on the frequency of mutations [20], the cells were synchronized and irradiated at the beginning of S-phase, then assayed for the frequency of selectable mutations in *HPRT*. As presented in Table I, the parental NF1604 cells and the derivative AS26 cells were irradiated with 8 J/m^2 $UV_{254nm,}$ which resulted in 30% survival of colony forming ability in NF1604 cells and 10% survival in the AS26 cells. In the NF1604 cells, we observed 32 mutant colonies, yielding a mutant frequency of 146 mutants per 10^6 clonable cells. In contrast, we observed only 3 mutant colonies in the AS26 population, which gave a mutant frequency of 6 mutants per 10^6 cells. This is a background frequency, which in this context is significant in light of the somewhat increased cytotoxicity the RAD18 knockdown cells. Cytotoxicity induced by genotoxins is well-established to be directly related to mutagenesis. The lowered survival of the AS26 cells would be expected to have resulted in higher mutation frequencies, but the opposite was observed. Similar experiments using different DNA damaging agents such as BPDE [26] on NF1604 and AS26 cells also showed a marked decrease in their mutagenic response. Repeated attempts to complement AS26 cells with RAD18-eGFP were unsuccessful, presumably because the antisense expression degraded the message. However, the reduction in UV mutagenesis can be inferred to be specific to the reduction in RAD18, since studies with clones that express the same construct but with more modest reductions in RAD18 (15%–50%) demonstrated mutant frequencies equal to the parental cells.

NIH-PA Author Manuscript

NIH-PA Author Manuscript

NIH-PA Author Manuscript

RAD18 is required for REV1 accumulation in nuclear foci

We hypothesized that one of the principal functions of RAD18 in human cells is to regulate the assembly of proteins required for translesion synthesis at blocked replication forks. If so, then REV1, which forms damage-induced nuclear foci [13;19] and is required for UV [17; 27] and BPDE [19] induced mutagenesis, will not relocalize in the absence of RAD18. We compared the mobility of REV1-eGFP in cells with greatly reduced RAD18 (AS26 cells) to that in wild-type NF1604 cells after UV damage. In cells expressing normal levels of RAD18, REV1 forms foci that colocalize with RAD18 within 4 h of exposure to 10 J/m^2 UV_{254nm}. REV1-eGFP within these foci is completely immobile (Fig. 5 line □). Under the same conditions, the percentage of RAD18 knockdown cells with REV1 foci did not increase after UV. (Fig. 5 line Δ) and the recovery of fluorescence is similar to that of the undamaged NF1604 cells (Fig. 5 line X). These results support the conclusion that RAD18 is required for recruitment of REV1 to damage-induced nuclear foci.

Discussion

Current models of DNA replication posit that the proteins necessary for this process are present in high local concentrations, suggesting that nuclear structural elements are required for the spatial and temporal coordination of these complicated processes [28]. These molecular machines are associated with the nuclear matrix, such that the DNA is pulled through the stationary complex. The proteins that comprise these complexes are located within preassembled replisomes, and as such represent subcellular organelles. In support of this concept, FRAP analysis of PCNA in cells in S-phase indicates a residence time of 30 min to several hours [29]. The question of whether Y-family DNA polymerases are present in such complexes, or are recruited when the fork is unable to bypass a helix-distorting lesion is an important question. Presumably the access of error-prone Y-family polymerases to primer termini is limited unless the fork is stalled. This would be accomplished by recruitment mechanisms. Indeed, the residence time of polη in replication foci of cells that have not been damaged is very short [30].

Foci are occasionally found in undamaged cells, but the nuclear distribution of Y-family polymerases in such cells is overwhelmingly diffuse. However, the distribution shifts to a focal pattern following UV irradiation [13;17] or exposure to BPDE [19;26]. This is especially dramatic when the population is enriched for cells entering S-phase [14], and the data presented here indicate that damage-induce nuclear foci are strictly S-phase-dependent. Damage-induced nuclear foci have been found to contain RAD18 and each of the Y-family DNA polymerases, including REV1 [9;19], polη [23;31;32], polι [31] and polκ [33].

To examine the nuclear dynamics of damage-induced focus formation, we studied the intracellular trafficking of RAD18 in response to DNA damage in living cells using fluorescence technologies. The subcellular localization and identification of the fusion protein in nuclear foci closely mimic the endogenous protein visualized with immunohistochemical techniques [26]. These observations strongly argue that examination of the dynamics of the fusion protein presents a valid model for studying the cell biology of RAD18 in living cells.

Our data indicate that RAD18-eGFP in the great majority of undamaged living human cells is found in the nucleus and the cytoplasm, and its nuclear distribution is diffuse in at least 95% of the cells. Studies of the diffusion of this protein in such cells indicate that most of the protein molecules are freely diffusible, as indicated by the recovery of fluorescence after photobleaching. This argues against the presence of RAD18 in large, preassembled DNA replication complexes. Obviously, we cannot exclude the possibility that a small proportion of the molecules are present in such complexes, as noted below.

NIH-PA Author Manuscript

NIH-PA Author Manuscript

NIH-PA Author Manuscript

Examination of the diffusion of the fusion protein in cells that have been irradiated but do not demonstrate a focal pattern showed that there was complete recovery of fluorescence that was indistinguishable from that in undamaged cells. Within 4h of irradiation, RAD18-eGFP relocalizes in a distinct focal pattern in the nucleus in at least 70% of cells in populations that have been enriched for S-phase. Strikingly, there is virtually no recovery of fluorescence when the proteins in these foci are photobleached (Fig. 2.). The diffusion coefficent of the protein in both circumstances was analyzed with sequential imaging of its movement in and out of a confocal plane using RICS technology. This methodology differs from FRAP in that the cell is not perturbed with a high-energy laser pulse, and the movement of the protein in and out of a confocal plane can be quantified over time. The mobility of RAD18 within the foci is reduced from ~13μm^2/sec to ~3μm^2/sec. These data are consistent with estimates of diffusion controlled processes within the nucleoplasm and with that of constrained cellular proteins [25], respectively. They support the hypothesis that RAD18 is recruited to DNA replication forks that have been stalled by the presence of photoproducts, and the protein becomes immobilized in the replication machinery under those circumstances. An interesting question is the function of the foci observed in the small percentage of cells that have not been exposed to UV, or that were exposed to UV in G_1 and analysed when the population is still in G_1 is unclear. We examined the fluorescence dynamics of the protein in this situation, and found that these parameters were indistinguishable in spontaneous and damage-induced foci. This means that RAD18 is immobilized and interacts with RAD6A and pol η in spontaneous foci, as it does in damage-induced foci. This small percentage the cells that appear to have preformed replisomes that include RAD18 may represent cells that are in S-phase despite the synchronization, which is determined to be 4% (Fig. 2A). It is possible that some of these cells are responding to replication-blocking spontaneous lesions, such as ethenoadenine

The REV1 protein is a Y-family DNA polymerase with deoxycytidyl transferase activity that is associated with translesion replication and first identified in budding yeast [34]. In that organism, REV1 is required for DNA damage tolerance and is epistatic to RAD18. The mechanism is poorly defined, but is independent of its catalytic function since a mutation in the N-terminal BRCT domain retains catalytic function but is deficient in mutagenesis. In human cells REV1 is also required for mutagenesis by UV [17;27] or BPDE [19] and the protein forms foci in the nuclei of cells that have been exposed to DNA damaging agents [13;19]. These foci colocalize with RAD18 and Y-family DNA polymerases, and are dependent on intact ubiquitin binding motifs in the REV1 protein [8;35]. The molecular mechanisms remain obscure, but it has been postulated that REV1 acts as a scaffold through interactions with other Y-family polymerases and DNA polymerase ζ. The regions of REV1 that are important for these interactions have been variously reported to be the N-terminal BRCT domain [36], the extreme C-terminus [12], or a region in the more proximal C-terminus [9]. Importantly, the latter authors found that REV1 is *not* epistatic to RAD18 in chicken DT40 cells, implying that they function independently.

To examine this question in human cells, we lowered RAD18 expression with the constitutive expression of antisense to RAD18 mRNA. Compared with parental wild-type cells, a derivative clone was identified in which the level of the protein was reduced by 85%. We confirmed that this reduction was functionally significant by examining UV-induced ubiquitination of PCNA and *HPRT* mutant frequencies induced by UV. There was a modest enhancement of cytotoxic responses and a significant reduction in the frequency of mutations induced by UV in cells with reduced RAD18. This is similar to mouse RAD18 −/− ES cells [37], but differs from DT40 RAD18−/− cells that are also sensitive to ionizing radiation [38]. There was no difference in induced mutagenesis in cells that expressed the antisense transcript but had a more modest reduction in RAD18 protein levels, arguing that the phenotype is not due to a nonspecific antisense effect.

NIH-PA Author Manuscript

NIH-PA Author Manuscript

NIH-PA Author Manuscript

Comparison of the localization of REV1-eGFP in living cells that had normal or reduced levels of RAD18 showed that RAD18 was required for the accumulation of REV1 in nuclear foci. In wild-type cells, REV1-eGFP forms foci after UV with frequencies that are similar to RAD18, and the proteins in these foci are immobile. In contrast, we were unable to detect REV1-containing foci in UV-irradiated cells that had reduced levels of RAD18. In those cells, nuclear REV1-eGFP remains in a diffuse pattern and is fully mobile regardless of UV-irradiation.

Examination of the association of RAD18 with RAD6A or polη with FLIM showed that energy transfer from RAD18-CFP to RAD6A-YFP or polη-YFP only occurred when the proteins were in damage-induced nuclear foci. This supports the argument that these proteins are not members of a preassembled replisome, but associate in response to signaling mechanisms that presumably derive from stalled replication forks. Watanabe et al. [23] made the interesting observation that RAD18 has a domain in the carboxy terminus that binds polη, and that deletion of this region prevents polη from forming foci in cells entering S-phase with DNA damage. These data raise the question of the relative importance of the physical association of the polymerase with RAD18 at the site of the stalled fork compared with the enhanced affinity of the polymerase for ubiquitinated PCNA. The FLIM data support a model in which physical association of these proteins occurs subsequent to DNA damage, but cannot address whether the association occurs as a result of enhanced affinity for ubiquitinated PCNA or conformationally altered RAD18, or both.

The unrestrained activity of error-prone DNA polymerases would clearly contribute to genomic instability, and there is considerable interest in the signaling mechanisms that control polymerase switching events. The data reported herein support a model in which RAD18 is recruited to stalled replication forks, implying that it is not a part of the replicative complex. Downstream events are presumed to involve signaling by RAD6-mediated ubiquitination, with PCNA a likely target [5;23]. We favor a model in which REV1 is recruited by ubiquitinated PCNA or other proteins, and then in turn acts as a scaffold for other TLS proteins. This model proposes that the principal role of RAD18 in human cells is to regulate TLS. The question of the requirement for RAD18 in homologous recombination in human cells remains open. It is likely that higher eukaryotes carry out RAD18-independent recombination, because mouse ES cells and chicken DT40 cells that are deficient in RAD18 have increased levels of sister chromatid exchange after exposure to mutagens. Rescue of blocked forks by strand invasion of the sister chromatid in higher eukaryotes may explain the relatively mild sensitivity of RAD18 knockouts to mutagen exposure compared with yeast.

Acknowledgements

The expertise of Dr. Enrico Gratton (University of California, Irvine) is central to the critical evaluation of these data, and we gratefully acknowledge his invaluable contribution to this work. We thank Mr. Tom Burke for excellent technical assistance and Dr. Suparna Mukhopadhyay for construction of the REV1 fusion expression plasmid.

This work was supported by grants from the National Aeronautics and Space Administration Ames Research Center NAG2-164-7 (WGM and BA), NIH CA112197 (WGM), the James Graham Brown Cancer Center (WGM) and by the Cell Migration Consortium PHSSUBUVGC 10641 (MD). The RICS and FLIM experiments reported in this paper were performed by NBW and MD at the Laboratory for Fluorescence Dynamics (LFD) at the University of California, Irvine (UCI). The LFD is supported jointly by the National Center for Research Resources of the National Institutes of Health (PHS 5 P41-RR003155) and UCI.

Reference List

1. Lawrence CW, Hinkle DC. DNA polymerase zeta and the control of DNA damage induced mutagenesis in eukaryotes. Cancer Surv 1996;28:21–31. [PubMed: 8977026]

NIH-PA Author Manuscript

NIH-PA Author Manuscript

NIH-PA Author Manuscript

2. Xiao W, Chow BL, Broomfield S, Hanna M. The Saccharomyces cerevisiae RAD6 group is composed of an error-prone and two error-free postreplication repair pathways. Genetics 2000;155:1633–1641. [PubMed: 10924462]
3. Lehmann AR, Niimi A, Ogi T, Brown S, Sabbioneda S, Wing JF, Kannouche PL, Green CM. Translesion synthesis: Y-family polymerases and the polymerase switch. DNA Repair (Amst) 2007;6:891–899. [PubMed: 17363342]
4. Goodman MF. Error-prone repair DNA polymerases in prokaryotes and eukaryotes. Annu Rev Biochem 2002;71:17–50. [PubMed: 12045089]
5. Hoege C, Pfander B, Moldovan GL, Pyrowolakis G, Jentsch S. RAD6-dependent DNA repair is linked to modification of PCNA by ubiquitin and SUMO. Nature 2002;419:135–141. [PubMed: 12226657]
6. Kannouche PL, Wing J, Lehmann AR. Interaction of human DNA polymerase eta with monoubiquitinated PCNA: a possible mechanism for the polymerase switch in response to DNA damage. Mol Cell 2004;14:491–500. [PubMed: 15149598]
7. Bienko M, Green CM, Crosetto N, Rudolf F, Zapart G, Coull B, Kannouche P, Wider G, Peter M, Lehmann AR, Hofmann K, Dikic I. Ubiquitin-binding domains in Y-family polymerases regulate translesion synthesis. Science 2005;310:1821–1824. [PubMed: 16357261]
8. Wood A, Garg P, Burgers PM. A ubiquitin-binding motif in the translesion DNA polymerase Rev1 mediates its essential functional interaction with ubiquitinated proliferating cell nuclear antigen in response to DNA damage. JBiol Chem 2007;282:20256–20263. [PubMed: 17517887]
9. Ross AL, Simpson LJ, Sale JE. Vertebrate DNA damage tolerance requires the C-terminus but not BRCT or transferase domains of REV1. Nucleic Acids Res 2005;33:1280–1289. [PubMed: 15741181]
10. Murakumo Y, Mizutani S, Yamaguchi M, Ichihara M, Takahashi M. Analyses of ultraviolet-induced focus formation of hREV1 protein. Genes Cells 2006;11:193–205. [PubMed: 16483309]
11. Murakumo Y, Ogura Y, Ishii H, Numata S, Ichihara M, Croce CM, Fishel R, Takahashi M. Interactions in the error-prone postreplication repair proteins hREV1, hREV3, and hREV7. JBiol Chem 2001;276:35644–35651. [PubMed: 11485998]
12. Guo C, Fischhaber PL, Luk-Paszyc MJ, Masuda Y, Zhou J, Kamiya K, Kisker C, Friedberg EC. Mouse Rev1 protein interacts with multiple DNA polymerases involved in translesion DNA synthesis. EMBO J 2003;22:6621–6630. [PubMed: 14657033]
13. Tissier A, Kannouche P, Reck MP, Lehmann AR, Fuchs RP, Cordonnier A. Co-localization in replication foci and interaction of human Y-family members, DNA polymerase pol eta and REVl protein. DNA Repair (Amst) 2004;3:1503–1514. [PubMed: 15380106]
14. Nakajima S, Lan L, Kanno S, Usami N, Kobayashi K, Mori M, Shiomi T, Yasui A. Replication-dependent and -independent responses of RAD18 to DNA damage in human cells. JBiol Chem 2006;281:34687–34695. [PubMed: 16980296]
15. Davies AA, Huttner D, Daigaku Y, Chen S, Ulrich HD. Activation of ubiquitin-dependent DNA damage bypass is mediated by replication protein a. Mol Cell 2008;29:625–636. [PubMed: 18342608]
16. Ouellette MM, McDaniel LD, Wright WE, Shay JW, Schultz RA. The establishment of telomerase-immortalized cell lines representing human chromosome instability syndromes. Hum Mol Genet 2000;9:403–411. [PubMed: 10655550]
17. Clark DR, Zacharias W, Panaitescu L, McGregor WG. Ribozyme-mediated REV1 inhibition reduces the frequency of UV-induced mutations in the human HPRT gene. Nucleic Acids Res 2003;31:4981–4988. [PubMed: 12930947]
18. Xin H, Lin W, Sumanasekera W, Zhang Y, Wu X, Wang Z. The human RAD18 gene product interacts with HHR6A and HHR6B. Nucleic Acids Res 2000;28:2847–2854. [PubMed: 10908344]
19. Mukhopadhyay S, Clark DR, Watson NB, Zacharias W, McGregor WG. REV1 accumulates in DNA damage-induced nuclear foci in human cells and is implicated in mutagenesis by benzo[a] pyrenediolepoxide. Nucleic Acids Res 2004;32:5820–5826. [PubMed: 15523096]
20. McGregor WG, Chen RH, Lukash L, Maher VM, McCormick JJ. Cell cycle-dependent strand bias for UV-induced mutations in the transcribed strand of excision repair-proficient human fibroblasts but not in repair-deficient cells. Mol Cell Biol 1991;11:1927–1934. [PubMed: 2005888]

NIH-PA Author Manuscript

NIH-PA Author Manuscript

NIH-PA Author Manuscript

21. Digman MA, Brown CM, Sengupta P, Wiseman PW, Horwitz AR, Gratton E. Measuring fast dynamics in solutions and cells with a laser scanning microscope. Biophys J 2005;89:1317–1327. [PubMed: 15908582]
22. Digman MA, Caiolfa VR, Zamai M, Gratton E. The phasor approach to fluorescence lifetime imaging analysis. Biophys J 2008;94:L14–L16. [PubMed: 17981902]
23. Watanabe K, Tateishi S, Kawasuji M, Tsurimoto T, Inoue H, Yamaizumi M. Rad18 guides poleta to replication stalling sites through physical interaction and PCNA monoubiquitination. EMBO J 2004;23:3886–3896. [PubMed: 15359278]
24. Masuyama S, Tateishi S, Yomogida K, Nishimune Y, Suzuki K, Sakuraba Y, Inoue H, Ogawa M, Yamaizumi M. Regulated expression and dynamic changes in subnuclear localization of mammalian Rad18 under normal and genotoxic conditions. Genes Cells 2005;10:753–762. [PubMed: 16098139]
25. Digman MA, Sengupta P, Wiseman PW, Brown CM, Horwitz AR, Gratton E. Fluctuation correlation spectroscopy with a laser-scanning microscope: exploiting the hidden time structure. Biophys J 2005;88:L33–L36. [PubMed: 15792971]
26. Watson NB, Mukhopadhyay S, McGregor WG. Translesion DNA replication proteins as molecular targets for cancer prevention. Cancer Lett 2006;241:13–22. [PubMed: 16303242]
27. Gibbs PE, Wang XD, Li Z, McManus TP, McGregor WG, Lawrence CW, Maher VM. The function of the human homolog of Saccharomyces cerevisiae REV1 is required for mutagenesis induced by UV light. Proc Natl Acad Sci USA 2000;97:4186–4191. [PubMed: 10760286]
28. Cook PR. The organization of replication and transcription. Science 1999;284:1790–1795. [PubMed: 10364545]
29. Leonhardt H, Rahn HP, Weinzierl P, Sporbert A, Cremer T, Zink D, Cardoso MC. Dynamics of DNA replication factories in living cells. J Cell Biol 2000;149:271–280. [PubMed: 10769021]
30. Solovjeva L, Svetlova M, Sasina L, Tanaka K, Saijo M, Nazarov I, Bradbury M, Tomilin N. High mobility of flap endonuclease 1 and DNA polymerase eta associated with replication foci in mammalian S-phase nucleus. Mol Biol Cell 2005;16:2518–2528. [PubMed: 15758026]
31. Kannouche P, Fernandez de Henestrosa AR, Coull B, Vidal AE, Gray C, Zicha D, Woodgate R, Lehmann AR. Localization of DNA polymerases eta and iota to the replication machinery is tightly co-ordinated in human cells. EMBO J 2003;22:1223–1233. [PubMed: 12606586]
32. Kannouche P, Broughton BC, Volker M, Hanaoka F, Mullenders LH, Lehmann AR. Domain structure, localization, and function of DNA polymerase eta, defective in xeroderma pigmentosum variant cells. Genes Dev 2001;15:158–172. [PubMed: 11157773]
33. Bi X, Barkley LR, Slater DM, Tateishi S, Yamaizumi M, Ohmori H, Vaziri C. Rad18 regulates DNA polymerase kappa and is required for recovery from S-phase checkpoint-mediated arrest. Mol Cell Biol 2006;26:3527–3540. [PubMed: 16611994]
34. Nelson JR, Lawrence CW, Hinkle DC. Deoxycytidyl transferase activity of yeast REV1 protein. Nature 1996;382:729–731. [PubMed: 8751446]
35. Guo C, Sonoda E, Tang TS, Parker JL, Bielen AB, Takeda S, Ulrich HD, Friedberg EC. REV1 protein interacts with PCNA: significance of the REV1 BRCT domain in vitro and in vivo. Mol Cell 2006;23:265–271. [PubMed: 16857592]
36. Jansen JG, Tsaalbi-Shtylik A, Langerak P, Calleja F, Meijers CM, Jacobs H, De Wind N. The BRCT domain of mammalian Rev1 is involved in regulating DNA translesion synthesis. Nucleic Acids Res 2005;33:356–365. [PubMed: 15653636]
37. Tateishi S, Niwa H, Miyazaki J, Fujimoto S, Inoue H, Yamaizumi M. Enhanced genomic instability and defective postreplication repair in RAD18 knockout mouse embryonic stem cells. Mol Cell Biol 2003;23:474–481. [PubMed: 12509447]
38. Szuts D, Simpson LJ, Kabani S, Yamazoe M, Sale JE. Role for RAD18 in homologous recombination in DT40 cells. Mol Cell Biol 2006;26:8032–8041. [PubMed: 16923963]

NIH-PA Author Manuscript

NIH-PA Author Manuscript

NIH-PA Author Manuscript

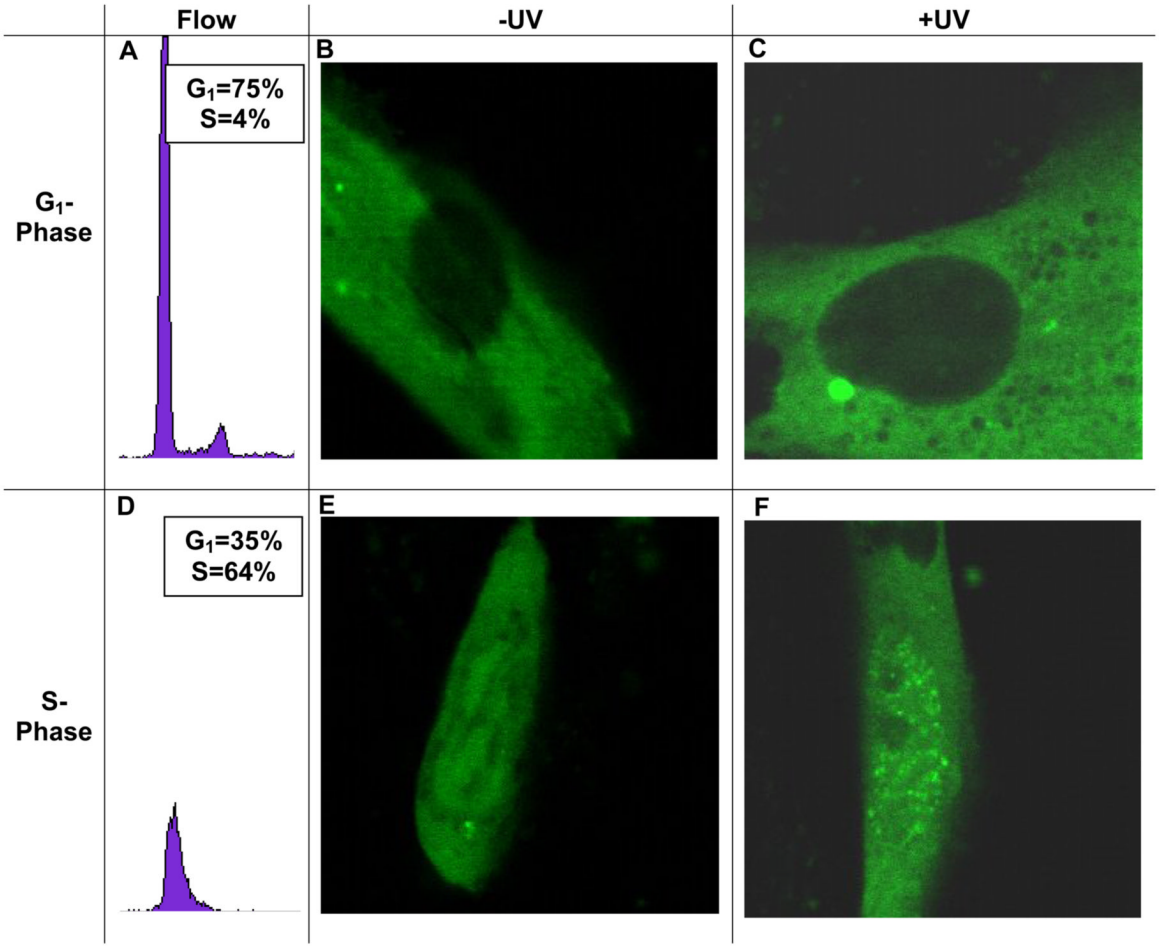

Cell cycle phase and treatment	Cells without foci	Cells with foci
G_1, no UV	>95%	<5%
G_1, with UV	>90%	<10%
S, no UV	>95%	<5%
S, with UV	<20%	>80%

Fig. 1.

Confocal microscopy images of RAD18-GFP. **A** and **D**, flow cytometry showing cells synchronized in G_1 and S-phase respectively. **B** and **C**, RAD18-GFP in G_1 phase, unirradiated and irradiated with 12 J/m^2 respectively. **E** and **F**, RAD18-GFP in S-phase, unirradiated and irradiated with 12 J/m^2 respectively. One hundred cells from populations exposed to one or the other of the four conditions were randomly inspected, and the table indicates the percentage of cells that exhibited foci.

NIH-PA Author Manuscript
NIH-PA Author Manuscript
NIH-PA Author Manuscript

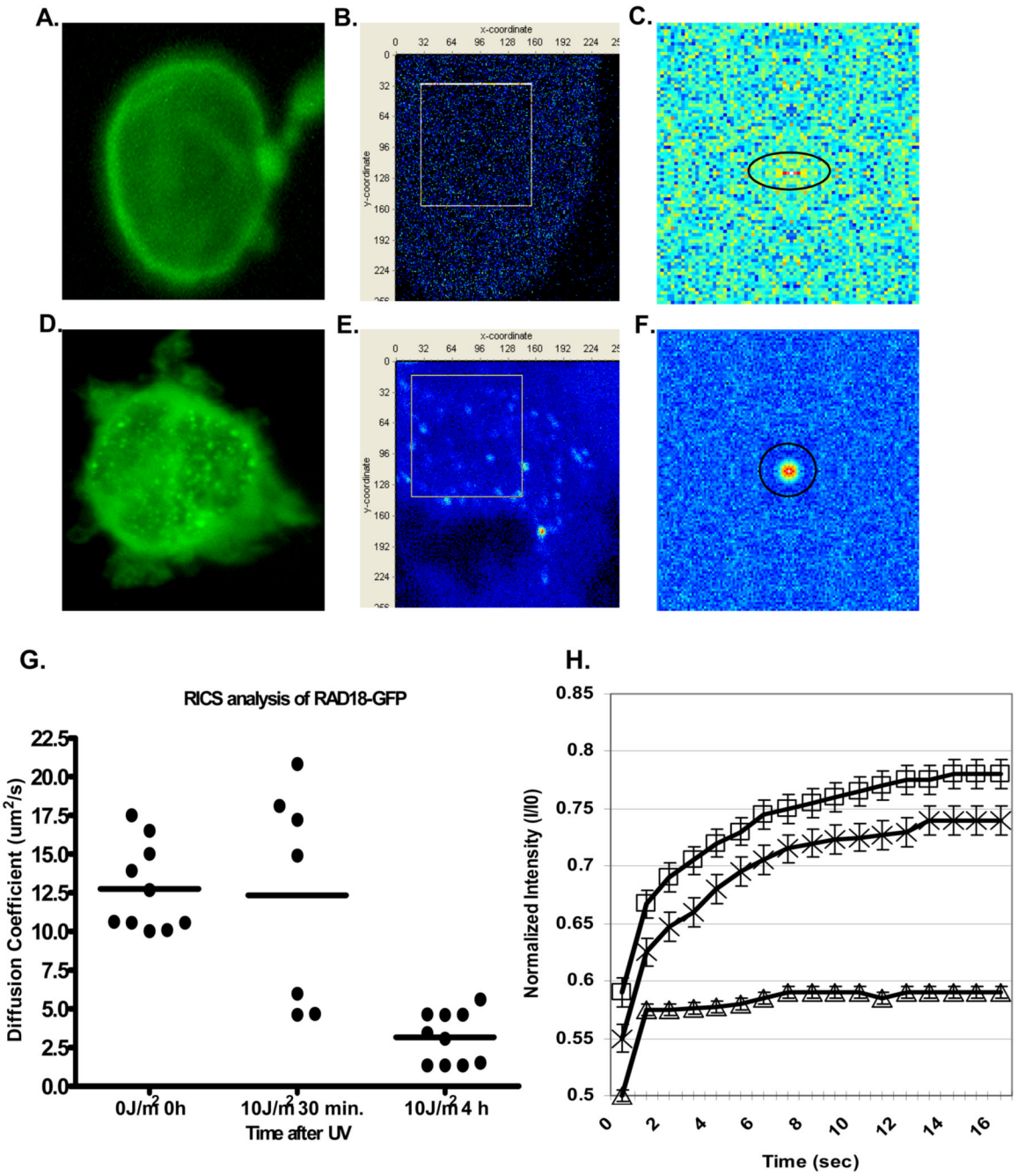

Fig. 2.

A, Typical fluorescent image of an undamaged cell expressing RAD18-eGFP. **B**, Raster scan image of RAD18-eGFP in unirradiated in NF1604 cells. The fusion protein is confined to the nucleus in a diffuse pattern. **D**, Typical fluorescent image of an irradiated cell expressing RAD18-eGFP. **E**, Raster scan image of RAD18-eGFP 4h after being exposed to 10 J/m^2 UV_{254nm}. Panels **C** and **F** are the 2D correlation maps for the images in panels **B** and **E** respectively. Fluorescence intensity is shown as red=higher intensity and blue=lower intensity. Panel **C** has correlation only in the x direction due to RAD18-eGFP being freely mobile in the absence of damage. Panel **F** has a more rounded shape in the 2D correlation map. This indicates correlation in both the x and y direction due to the relative immobility of the foci once bound

NIH-PA Author Manuscript

NIH-PA Author Manuscript

NIH-PA Author Manuscript

to damaged DNA. **G**, graph with diffusion coefficients of cells randomly chosen from separate high-power fields. The average diffusion coefficient is 12.8 μm^2/sec in unirradiated cells. Four hours after UV, when most cells demonstrated a focal pattern, RAD18-eGFP showed a 75% reduction in the diffusion coefficient (3.2 μm^2/s), consistent with immobilization ($P<.01$). Thirty minutes after UV treatment, the mean diffusion coefficient was 12.3 μm^2/sec. This was not a significant difference ($P>.05$). **H**, FRAP analysis of cells transfected with hRAD18-eGFP. Cells were irradiated with 10 J/m^2. Data derived from unirradiated cells are presented in the top line (□). The data in the middle line (X) are derived from UV-treated cells that were irradiated but did not form foci. Although the initial fluorescence intensity (I_0) of these cells at the time of the photobleaching pulse was lower, which reduced the I/I_0, the rate of recovery was indistinguishable from the unirradiated cells. These data indicate that UV-irradiation *per se* does not immobilize RAD18. Data in the lower line (Δ) were derived from cells that formed foci. The data shown were obtained from foci, and illustrate that RAD18 is unable to redistribute in this situation presumably because it is immobilized in a complex.

NIH-PA Author Manuscript

NIH-PA Author Manuscript

NIH-PA Author Manuscript

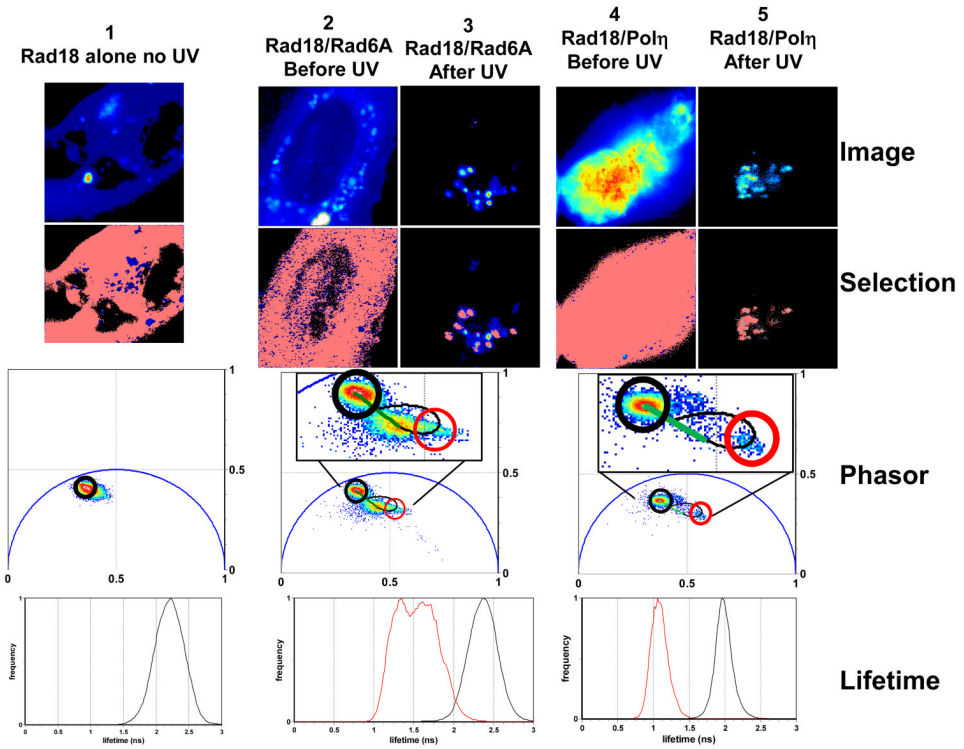

Fig. 3.

Upper row: cells expressing RAD18-CFP alone without irradiation (1), co-expressing RAD6A-YFP before UV irradiation (2), RAD-6A after UV irradiation (3), polη-YFP before irradiation (4) and polη after UV irradiation (5). The second row shows the pixels of the cells painted according to the selection (black and black circles, for the right and left image, respectively) of the phasor plot regions shown in row 3. The phasor plot contains the phasor of both cells (with and without irradiation). The irradiation produces shortening of the lifetime as show in row 4, which report the histogram of pixel lifetime (average) values and clustering of the phasors in two distinct regions. When the phasors in these regions are selected by the circular cursors, the pixels in the image corresponding to these phasors are highlighted as shown in the second row. The pixels with shorter lifetime (phasors selected by the red circle) correspond to specific punctuations in the image. The insets in row 3 show the details of the phasor plot with a green line joining the phasor of the donor and the phasor of the autofluorescence and the black ellipsoidal trajectory is the loci of the possible phasors with different FRET efficiencies. The red circle corresponds to 72% FRET efficiency for both constructs.

NIH-PA Author Manuscript

NIH-PA Author Manuscript

NIH-PA Author Manuscript

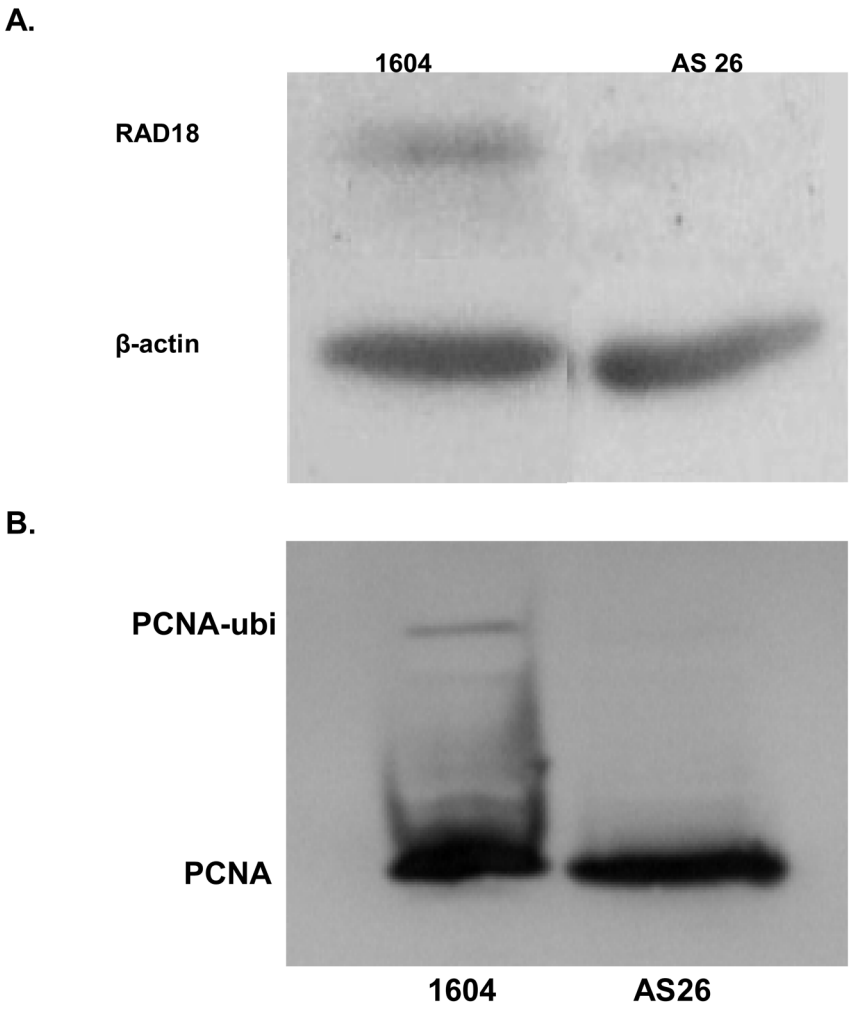

Fig. 4.

A. Western blot analysis of RAD18 levels in NF1604 cells and a derivative clone that expresses antisense RNA to RAD18 (AS26). RAD18 protein levels in AS26 was only 15% of that in the parental line, normalized to β-actin. **B.** Western blot analysis of PCNA 8 hrs after 15 J/m^2 UV_{254nm} in NF1604 cells and RAD18-reduced AS26 cells. Thirty micrograms of total cell lysate were loaded in both lanes. The higher molecular weight band represents monoubiquitinated PCNA, which was undetectable in AS26. Ubiquitinated PCNA was not detected in the absence of DNA damage in either cell line.

NIH-PA Author Manuscript

NIH-PA Author Manuscript

NIH-PA Author Manuscript

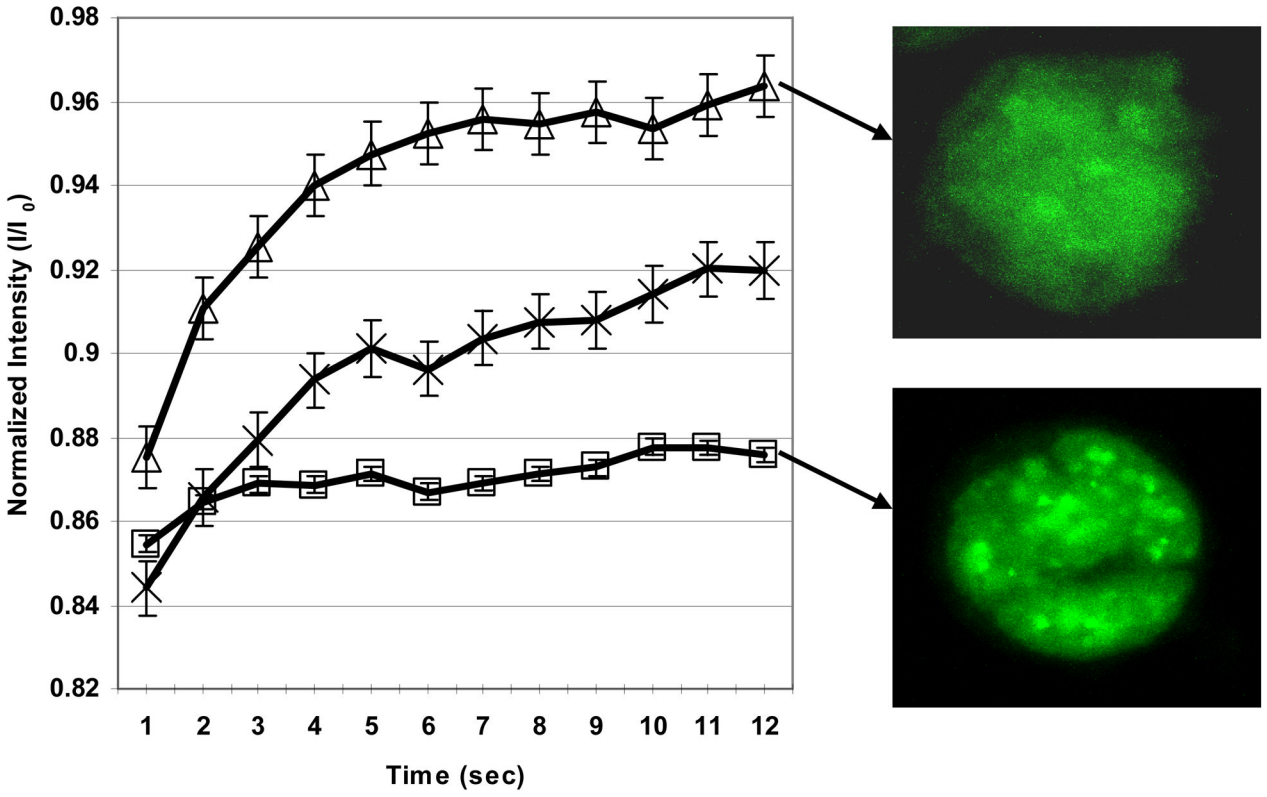

Fig 5.

Focal nuclear localization of REV1 is dependent on RAD18. FRAP measurements were made as in Fig. 1H. Each data point is the mean fluorescence intensity of at least 10 cells, and bars represent the standard deviation of the mean. The top line (Δ) is the recovery of REV1-eGFP in undamaged NF1604 cells, and represents the mobility of the fusion protein in the nucleus. The REV1-eGFP is in a focal nuclear pattern in approximately 50% of NF1604 cells 6 h after UV. The REV1 fusion protein in such foci is immobilized, indicated by the lack of recovery after photobleaching (bottom line □). In contrast, REV1-eGFP did not form foci after UV in AS26 cells (top line Δ), which have greatly reduced levels of RAD18. The ratio of fluorescence recovery of nuclear REV1 (I/I_0=0.09) in these cells is nearly identical from the ratio observed in NF1604 cells that were undamaged (0.08) (middle line X). The ratio for REV1 in NF1604 cells after damage was 0.02. Undamaged AS26 cells show an identical fluorescent redistribution pattern to that of the undamaged NF1604 cells (data not shown). A typical fluorescent image of REV1-eGFP localization in AS26 cells (top image) and 1604 cells (bottom image) after UV exposure is also shown.

NIH-PA Author Manuscript
NIH-PA Author Manuscript
NIH-PA Author Manuscript

Table I

UV-induced cytotoxicity and mutagenicity in synchronous populations of fibroblasts irradiated at the beginning of S-phase

Cell Line	UV Dose	%S	Mut. Clones Observed	# Cells Assayed in 6-TG (× 10^6)	Mut. Freq. (× 10^6)[a]
1604	0 J/m^2	100%	0	1	<10
1604	8J/m^2	30%	32	1	146
AS26	0 J/m^2	100%	0	1	<10
AS26	8 J/m^2	10%	3	2	6

[a]The mutant frequency is defined as mutants per 10^6 clonable cells. The number of observed mutants is corrected for cloning efficiency on the day of selection. These values ranged from 22 to 26%.